

Supplementary Information

A pillar[5]arene- and calix[4]pyrrole-based supramolecular polymer for selective removal of naphthols from water

Deniz Memis,^a Saide Akin,^a and Abdullah Aydogan^{a,b,*}

^a Department of Chemistry, Istanbul Technical University, Maslak, 34469, Istanbul, Türkiye

^b Department of Nanoscience and Nanoengineering, Istanbul Technical University, Maslak, 34469
Istanbul, Türkiye

*Corresponding author e-mail: aydoganab@itu.edu.tr

Table of Contents

General Considerations	2
Experimental	2
Synthesis of 3	3
Synthesis of 4	3
Synthesis of 1	4
Synthesis of 7	6
Synthesis of 2	8
NMR and FTIR Spectra	10
Surface Area and Porosity Analysis	16
Micropollutant Removal	17
Adsorption experiments	17
Removal efficiency	17
Adsorption kinetics	18
Adsorption isotherms	23
Binary-Component Adsorptions	24
References	25

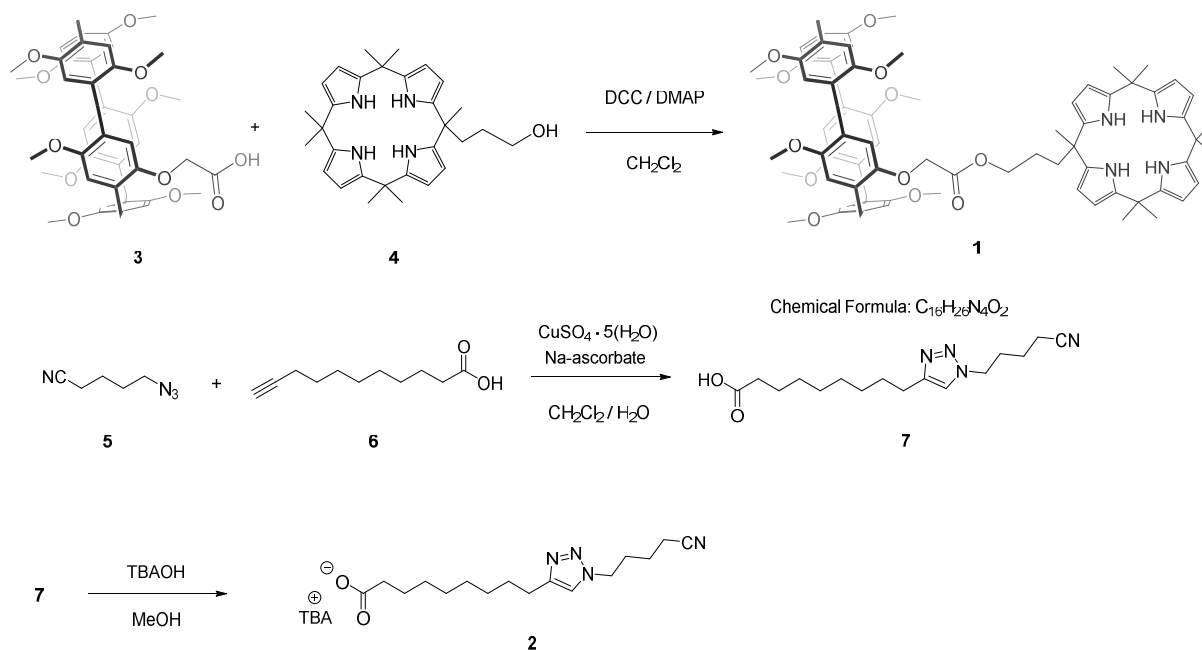
General Considerations

All reagents and solvents were acquired from commercial suppliers and used as received, unless otherwise specified. Pollutant solutions were prepared with deionized water at neutral pH. Column chromatography was performed over silica gel.

^1H -, NEOSY-, COSY-, and DOSY-NMR spectra were recorded on Agilent VNMRs 500 spectrometers using TMS as an internal reference at 25 °C. Mass spectra were measured on a Thermo Scientific Thermo Q Exactive HR mass spectrometer equipped with a LC unit. Melting points were determined using a Stuart SMP10 instrument with 1 °C min⁻¹ temperature increment under ambient conditions. SEM analyses were carried out by using FEI QuantaFEG 250 SEM instrument in ESEM mode or using Tescan Vega 3 instrument. XRD measurements were carried out with a PANalytical X'Pert PRO instrument equipped with Cu K α X-Ray source at 1.5406 Å wavelength and 3°/min scan rate. FTIR spectra were collected on a Perkin Elmer FT-IR Spectrum One spectrometer. Stereomicroscope imaging was conducted by using a Discovery V20 microscope equipped with an AxioCam ICc 1 digital camera system. Surface area and pore size analyses were carried out with a Quantachrome Autosorb iQ instrument.

Compounds **3**,¹ **4**,² and **5**³ were prepared according to previous literature procedures.

Experimental



Synthesis of **3**

Compound **3** was synthesized similar to a previously reported procedure as a white powder with 27% yield.¹

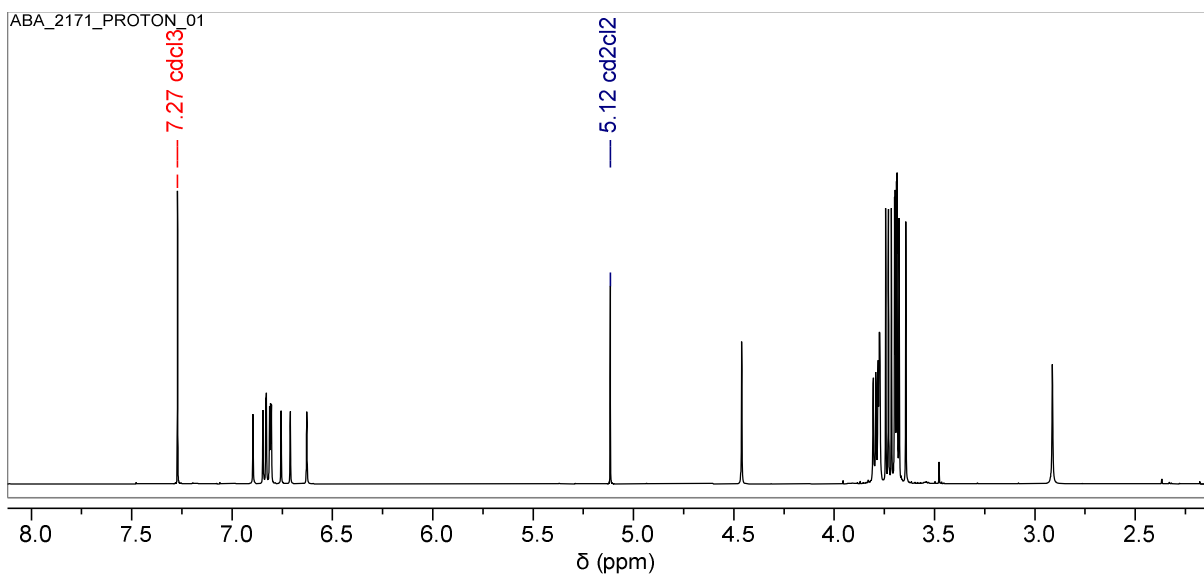


Figure S1. ¹H NMR spectrum of **3** recorded in CDCl₃ (500 MHz, 25 °C).

Synthesis of **4**

Compound **4** was prepared based on our previously published procedure.²

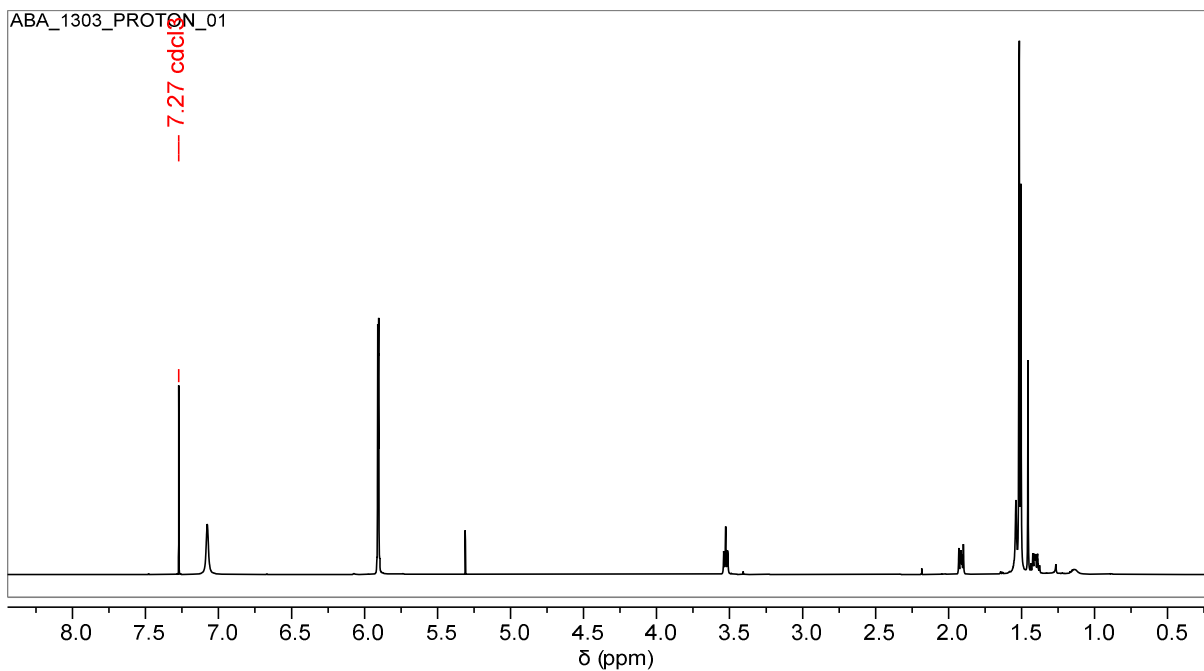


Figure S2. ¹H NMR spectrum of **4** recorded in CDCl₃ (500 MHz, 25 °C).

Synthesis of **1**

A mixture of **3** (2.0 g, 2.52 mmol), **4** (1.08 g, 2.29 mmol), and DMAP (28.2 mg, 0.23 mmol) in methylene chloride (45 mL) was heated in a Schlenk tube to obtain a clear solution. DCC (524 mg, 2.52 mmol in 5 mL CH₂Cl₂) was then added dropwise in to the mixture. The final reaction mixture was allowed to stir for 72 h under N₂ atmosphere. Once completed, the reaction mixture was washed sequentially with (i) HCl solution (50 mL, 0.2 N), (ii) saturated NaHCO₃ solution (50 mL), and (iii) distilled water (50 mL) twice. After drying the organic phase with anhydrous Na₂SO₄, CH₂Cl₂ was evaporated under reduced pressure. TLC analysis of the crude mixture revealed R_f value of 0.32 for the product when DCM was used as mobile phase. Column chromatography (silica gel, CH₂Cl₂ eluent) afforded compound **1** as a white solid (1.60 g, 56%). ¹H NMR (500 MHz, CDCl₃) δ = 7.08 (s, 2H, NH), 7.06 (s, 2H, NH), 6.94 (s, 1H, CH), 6.82-6.78 (m, 8H, CH), 6.72 (s, 1H, CH), 5.92-5.89 (m, 8H, pyrrole-CH), 4.45 (s, 2H, -CH₂-), 4.09 (t, *J* = 6.7 Hz, 2H, -CH₂-), 3.86 (s, 2H, -CH₂-), 3.79 (m, 6H, -CH₂-), 3.76 (s, 2H, -CH₂-), 3.68-3.65 (m, 27H, -OCH₃), 1.92-1.89 (m, 2H, -CH₂-), 1.53-1.51 (m, 20H, -CH₃), 1.46 (s, 3H, -CH₃) ppm. ¹³C NMR (126 MHz, CDCl₃) δ = 169.3, 151.5, 150.9, 150.8, 149.0, 138.8, 138.6, 138.4, 136.7, 129.0, 128.2, 128.1, 128.0, 115.4, 114.2, 114.1, 113.9, 103.9, 102.9, 102.8, 69.8, 66.5, 65.3, 55.8, 55.7, 55.6, 53.1, 38.5, 36.8, 35.2, 29.8, 29.6, 29.3, 29.2, 29.0, 26.2, 23.9, 18.9 ppm. HRMS (ESI): *m/z* calcd for C₇₆H₉₂N₅O₁₂ [M+NH₄]⁺: 1266.67425; found: 1266.67189.

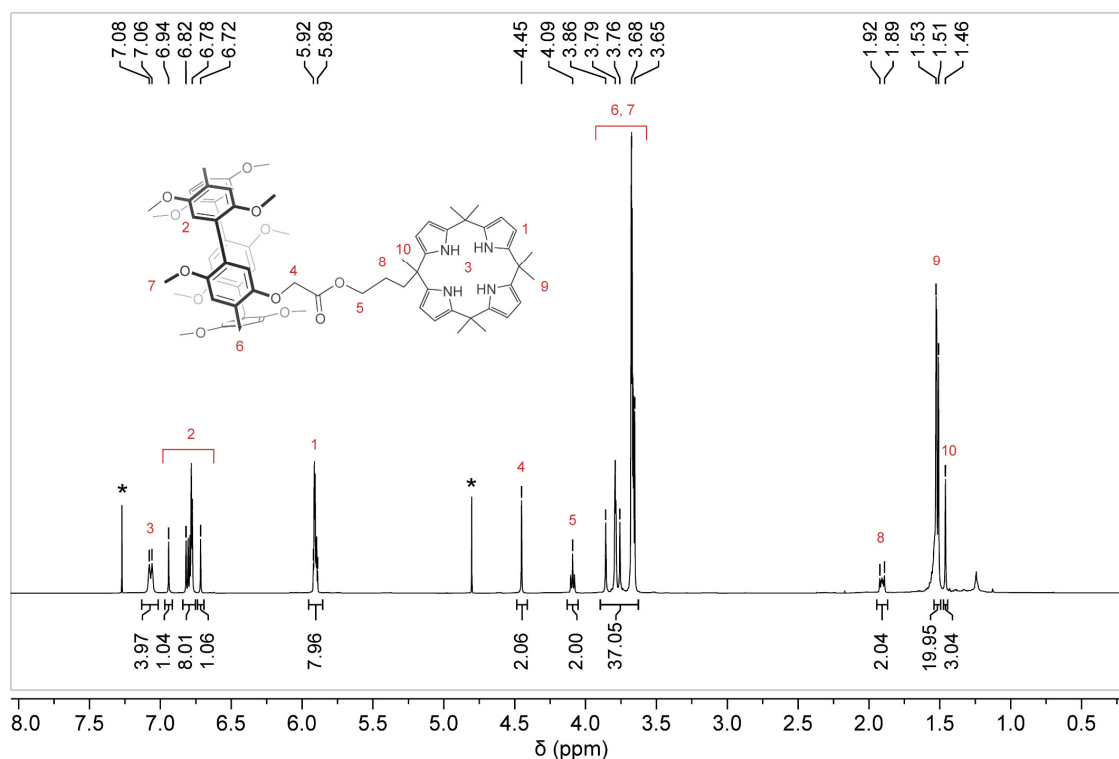


Figure S3. ¹H NMR spectrum of **1** recorded in CDCl₃ (500 MHz).

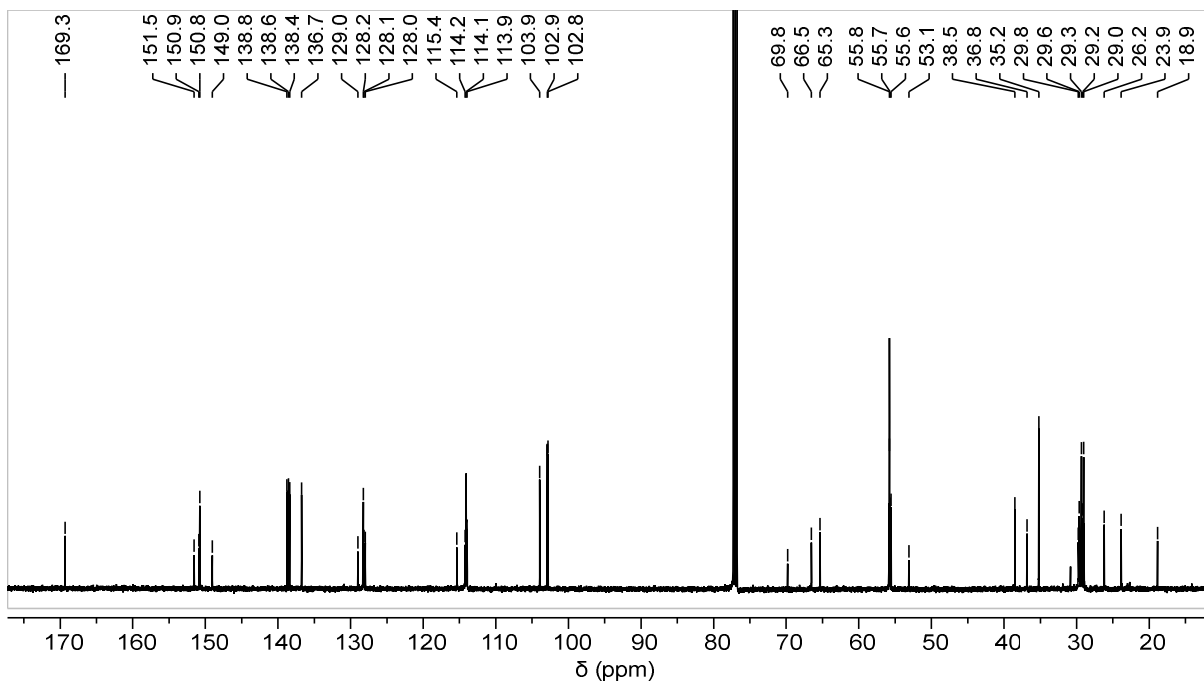


Figure S4. ^{13}C NMR spectrum of **1** recorded in CDCl_3 (126 MHz).

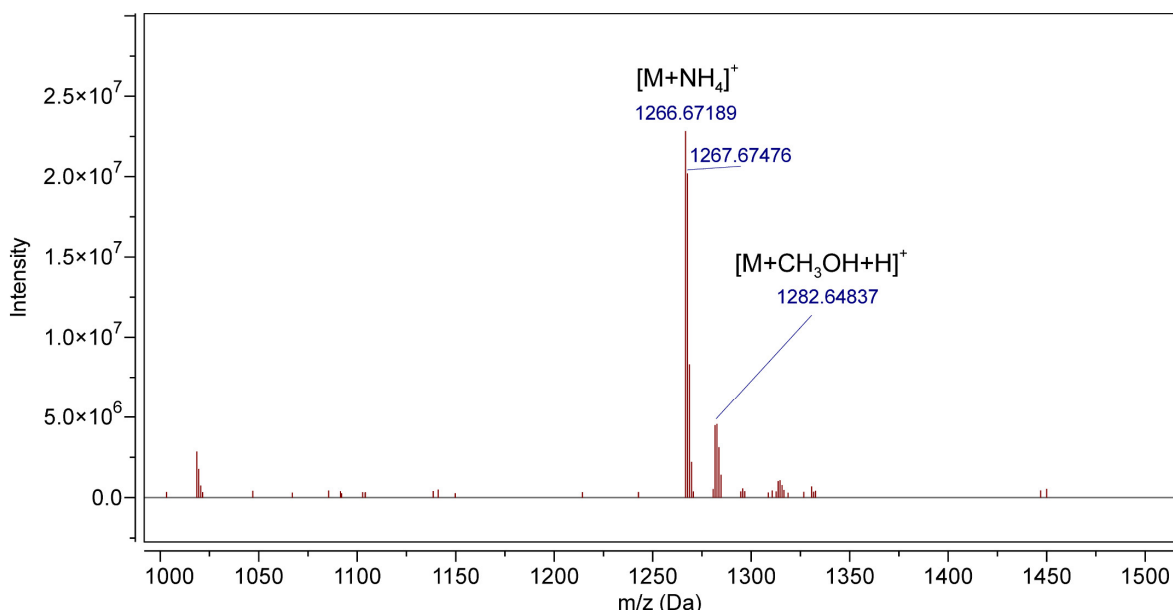


Figure S5. HR-ESIMS spectrum of **1**.

Synthesis of 7

To a 4 mL CH₂Cl₂ solution of 5-azidopentanenitrile (220 mg, 1.77 mmol) and 10-undecynoic acid (363 mg, 1.95 mmol), 4 mL distilled water was added. Then, sodium ascorbate (421 mg, 2.13 mmol) and CuSO₄·(H₂O)₅ (177 mg 0.71 mmol) were added in one portion to the aqueous phase. The final mixture was stirred at rt for 48 h under N₂ atmosphere. After completion, the reaction mixture was diluted with 50 mL CH₂Cl₂ and washed with acetic acid (0.2 M, 4 × 30 mL) and water (4 × 10 mL). Organic phase was then dried over anhydrous Na₂SO₄, and the solution was concentrated under reduced pressure. Precipitation into hexane afforded a white solid (358 mg, 66%). M.p. 71-73 °C. ¹H NMR (500 MHz, CDCl₃) δ = 7.31 (s, 1H), 4.40 (t, *J* = 6.8 Hz, 2H), 2.76 – 2.69 (m, 2H), 2.41 (t, *J* = 6.9 Hz, 2H), 2.35 (t, *J* = 7.5 Hz, 2H), 2.14 – 2.04 (m, 2H), 1.74 – 1.60 (m, 6H), 1.40 – 1.30 (m, 8H). ¹³C NMR (126 MHz, CDCl₃) δ = 178.8, 148.6, 120.7, 119.0, 49.1, 34.0, 29.3, 29.0, 28.9, 25.4, 24.7, 22.3, 16.7 ppm. HRMS (ESI): *m/z* calcd for C₁₆H₂₇N₄O₂ [M+H]⁺: 307.21285; found: 307.21289.

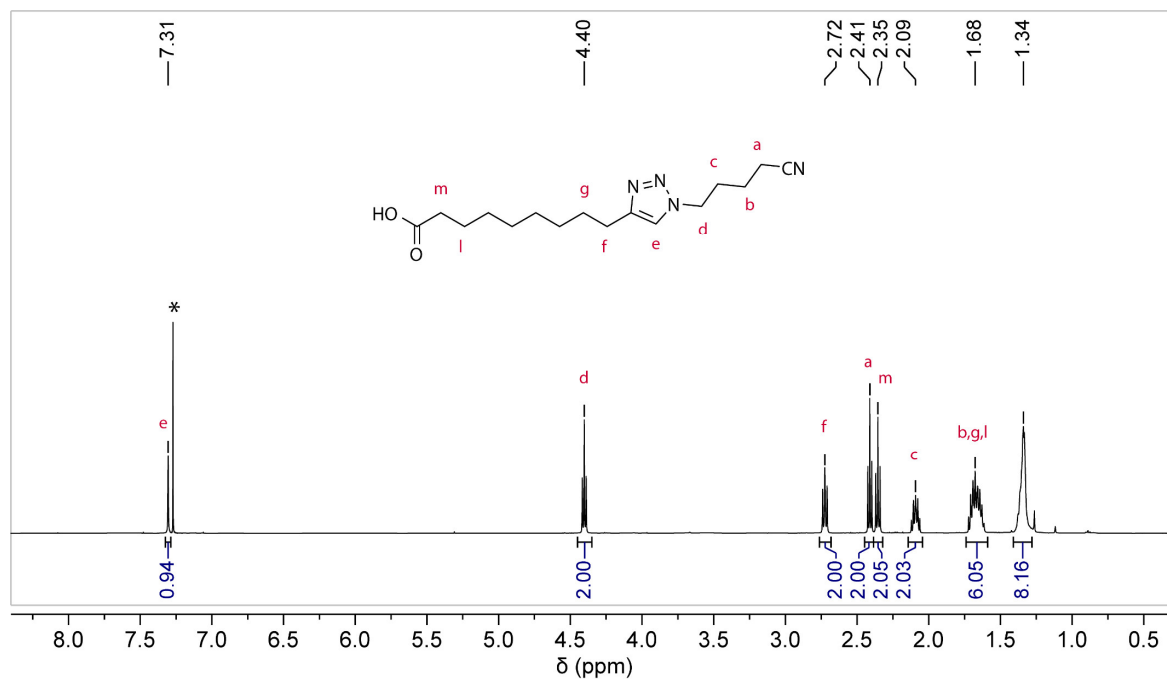


Figure S6. ¹H NMR spectrum of 7 recorded in CDCl₃ (500 MHz).

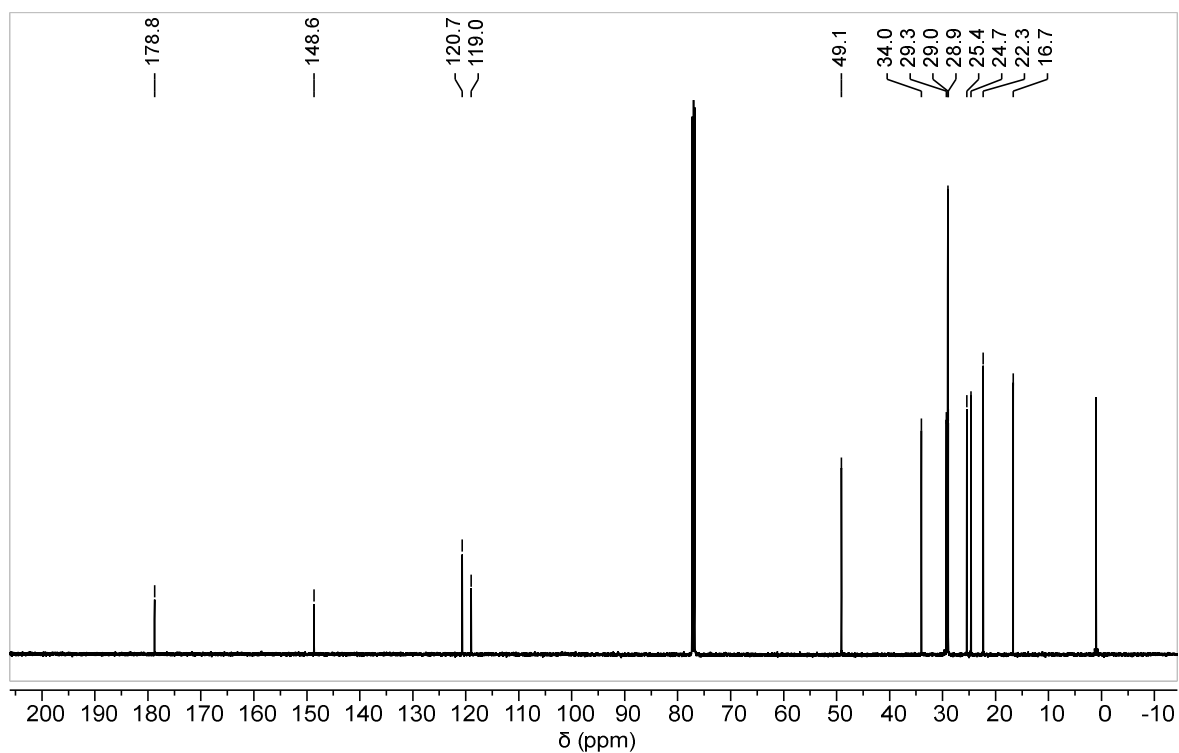


Figure S7. ^{13}C NMR spectrum of **7** recorded in CDCl_3 (126 MHz).

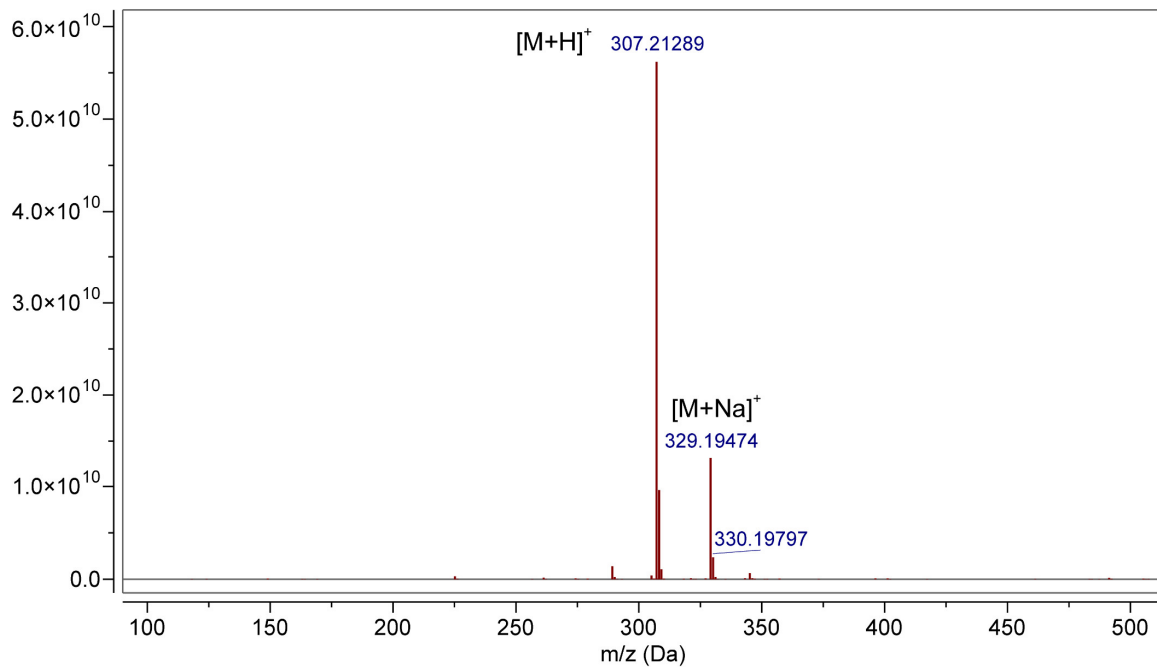


Figure S8. HRMS (ESI) spectrum of **7**.

Synthesis of **2**

To a CHCl₃ solution (2 mL) of **7** (33 mg, 0.11 mmol), isopropyl alcohol solution of tetrabutylammonium hydroxide (TBAOH) (106 mM, 1 mL) was added dropwise. The reaction mixture was stirred at room temperature for 20 min. Removal of solvent followed by drying under vacuum afforded **2** quantitatively as a colorless sticky liquid. ¹H NMR (500 MHz, CDCl₃) δ 7.33 (s, 1H), 4.37 (t, *J* = 6.8 Hz, 2H), 3.31 – 3.24 (m, 8H), 2.66 (t, *J* = 7.7 Hz, 2H), 2.39 (t, *J* = 7.0 Hz, 2H), 2.17 – 2.12 (m, 2H), 2.10 – 2.00 (m, 2H), 1.72 – 1.51 (m, 14H), 1.41 (h, *J* = 7.4 Hz, 8H), 1.28 (m, 8H), 0.98 (t, *J* = 7.3 Hz, 12H) ppm. ¹³C NMR (126 MHz, CDCl₃) δ = 179.3, 148.7, 120.7, 119.1, 58.7, 48.9, 38.1, 29.7, 29.4, 29.3, 29.2, 29.1, 29.1, 26.6, 25.6, 24.0, 22.3, 19.7, 16.6, 13.7 ppm. HRMS (ESI): *m/z* calcd for C₁₆H₂₅N₄O₂[−] [M-TBA][−]: 305.19830; found: 305.19809.

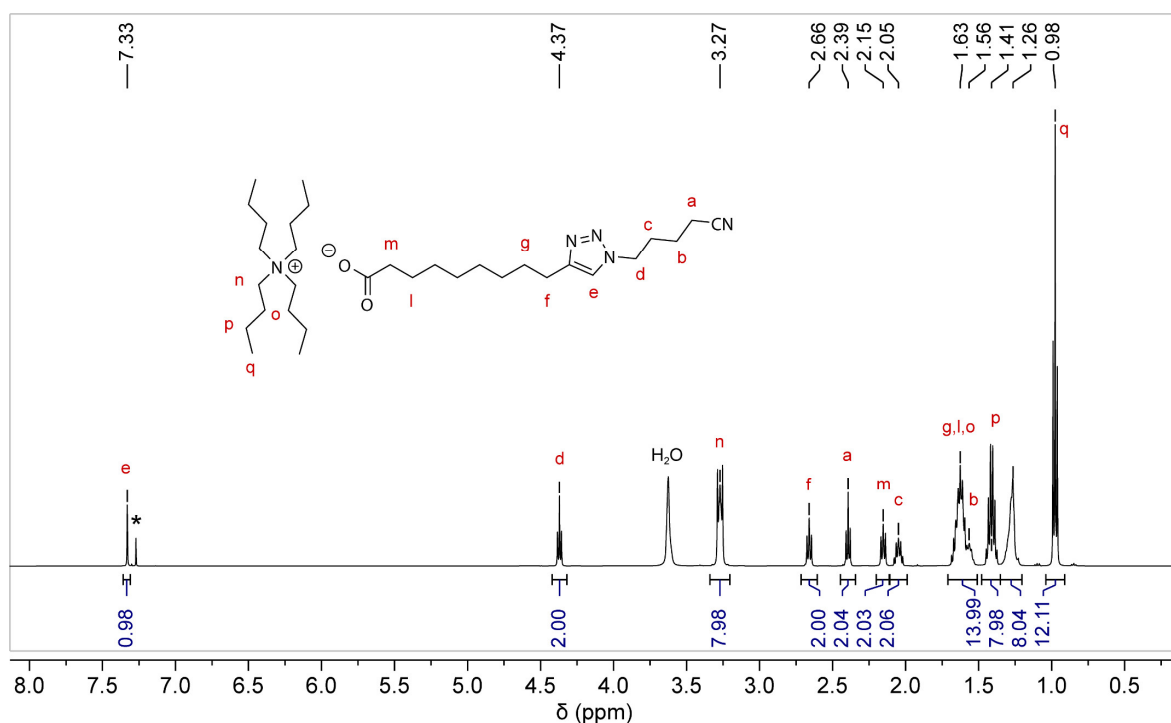


Figure S9. ¹H NMR spectrum of **2** recorded in CDCl₃ (500 MHz).

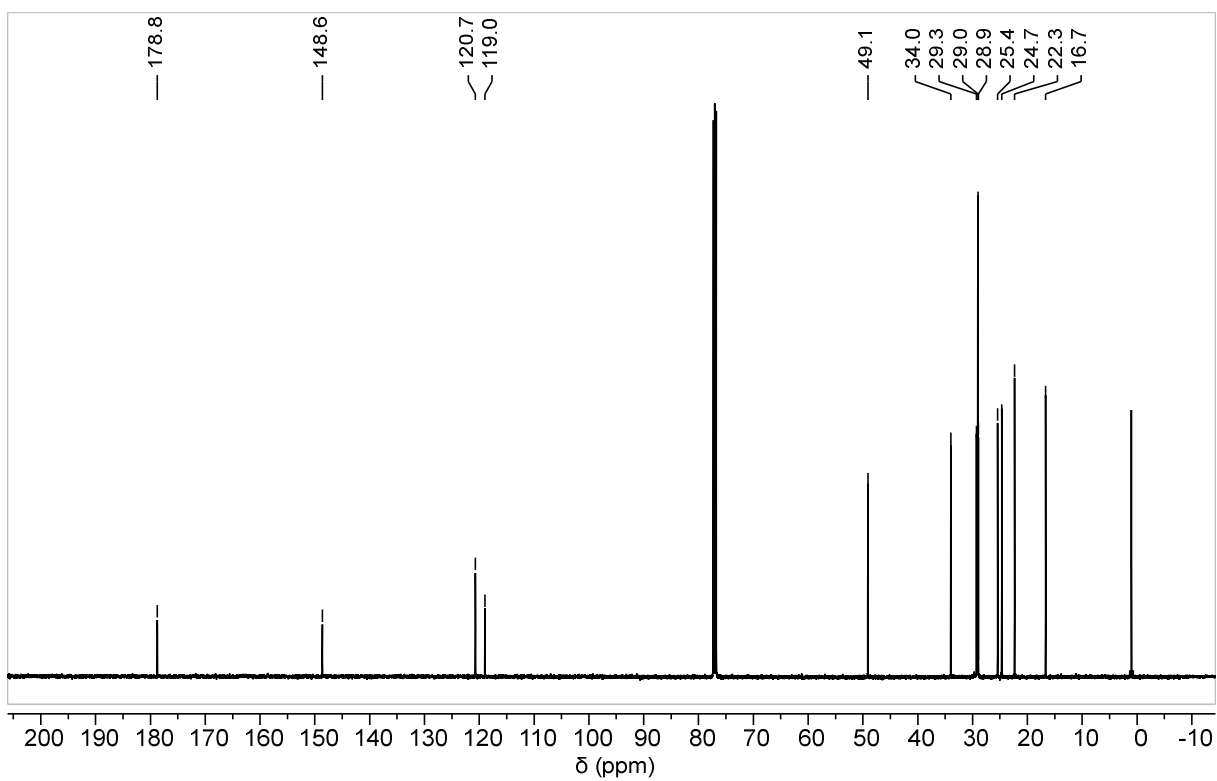


Figure S10. ^{13}C NMR spectrum of **2** recorded in CDCl_3 (126 MHz).

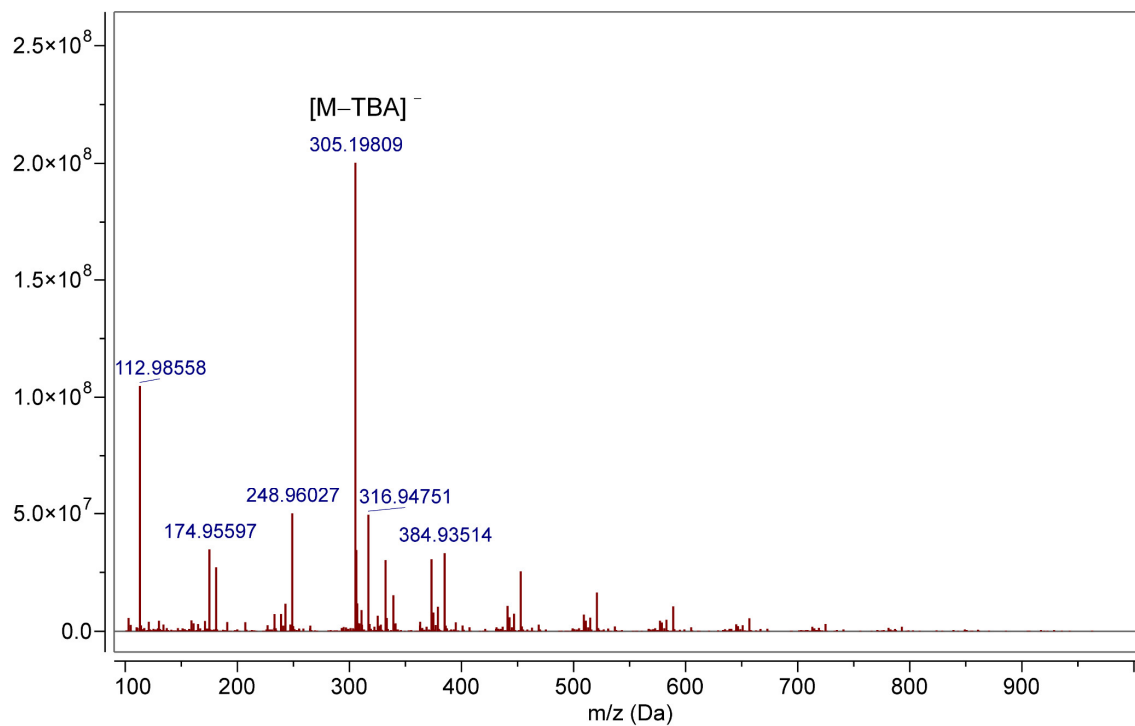


Figure S11. HRMS (ESI) spectrum of **2** recorded in negative ionization mode.

NMR and FTIR Spectra

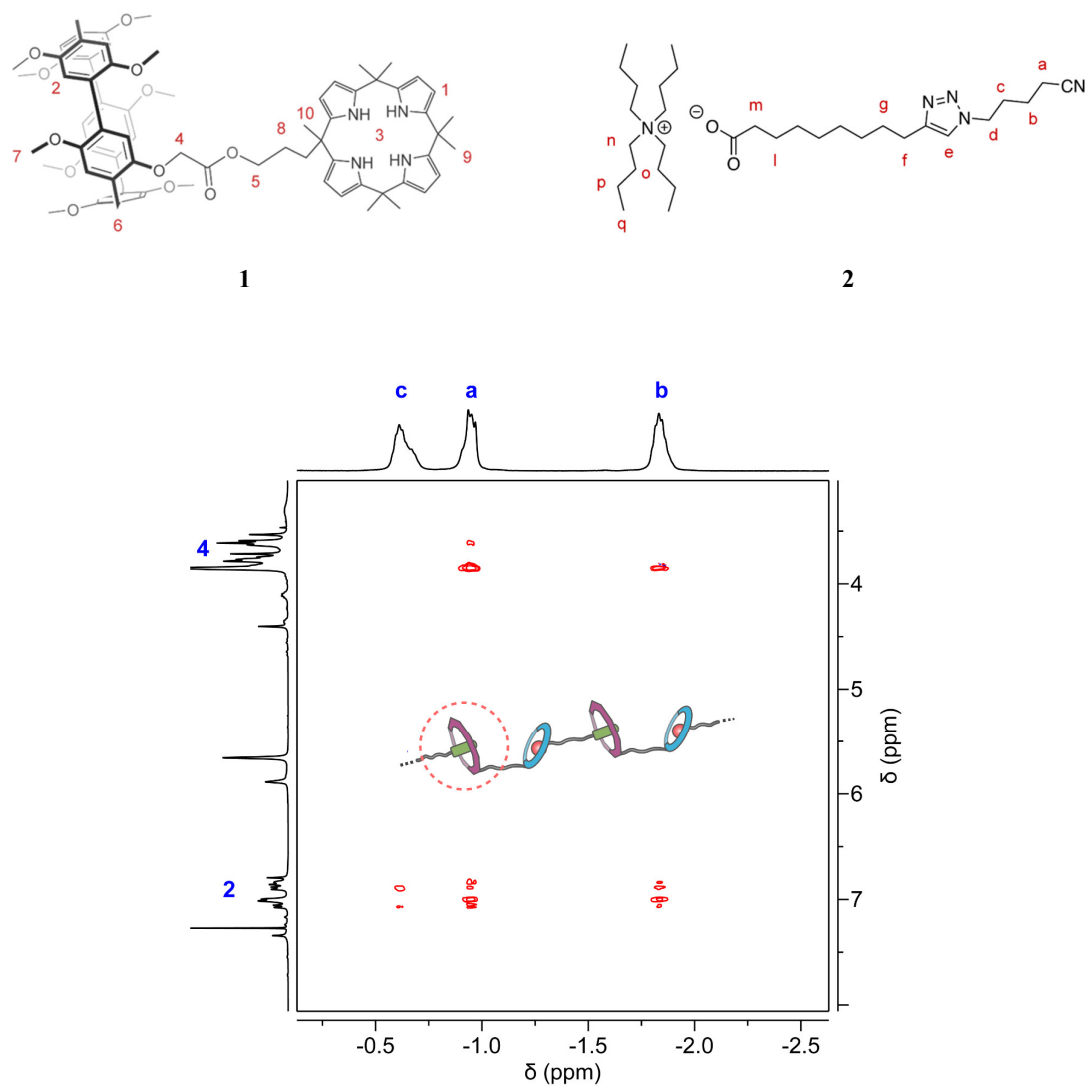


Figure S12. Partial NOESY spectrum of **SP** recorded in CDCl₃ (500 MHz) at 25 °C. The correlation peaks indicate the inclusion of alkylnitrile unit of guest **2** into the P5A segment of host **1**.

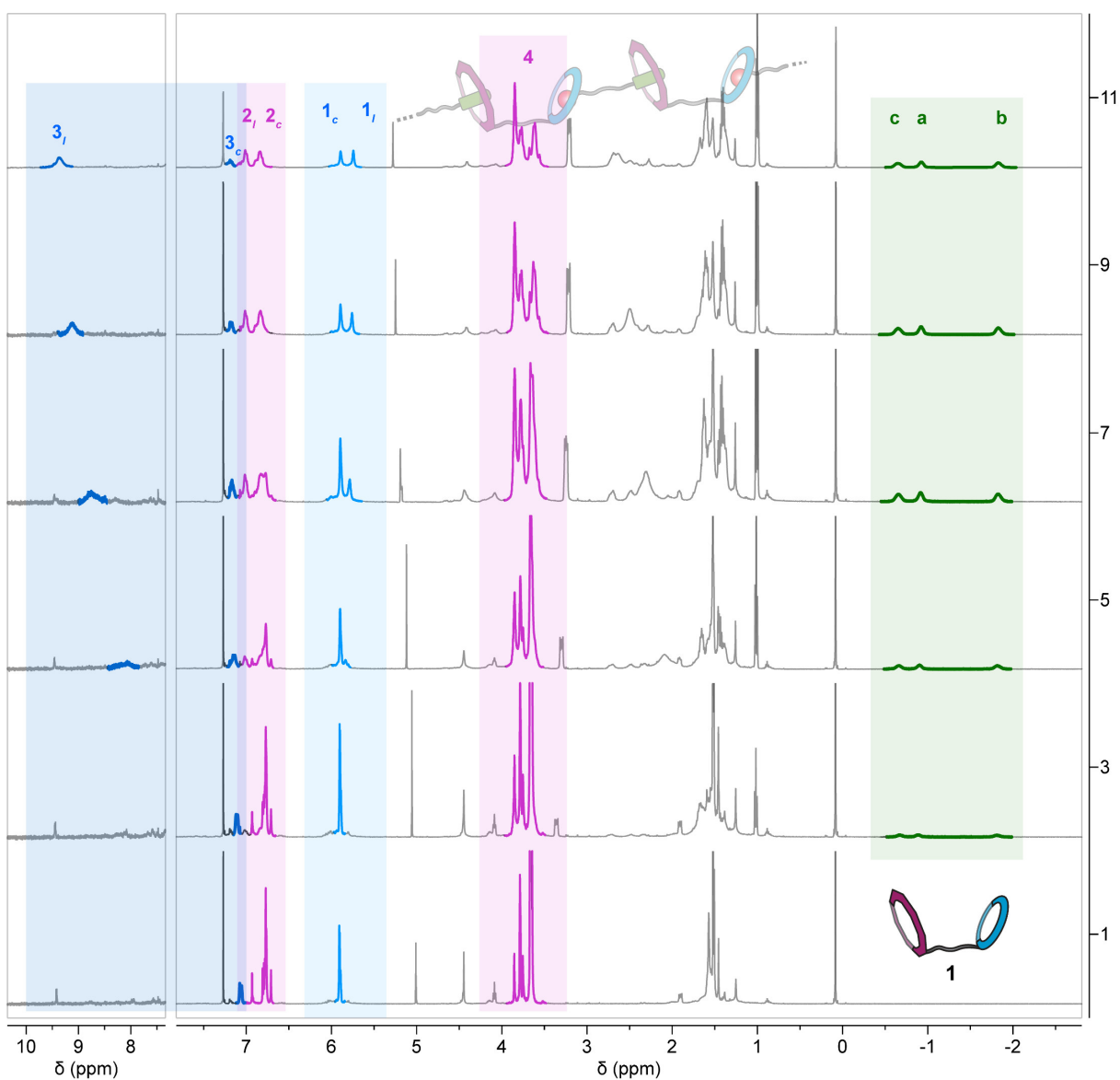


Figure S13. ^1H NMR spectra recorded in CDCl_3 (500 MHz) showing the changes on C4P, P5A, and alkylnitrile peaks during the titration of **1** (10 mM) with incremental amount of **2**. From bottom to top the equivalent of **2** increases in the order of 0.0, 0.2, 0.4, 0.6, 0.8, and 1.0.

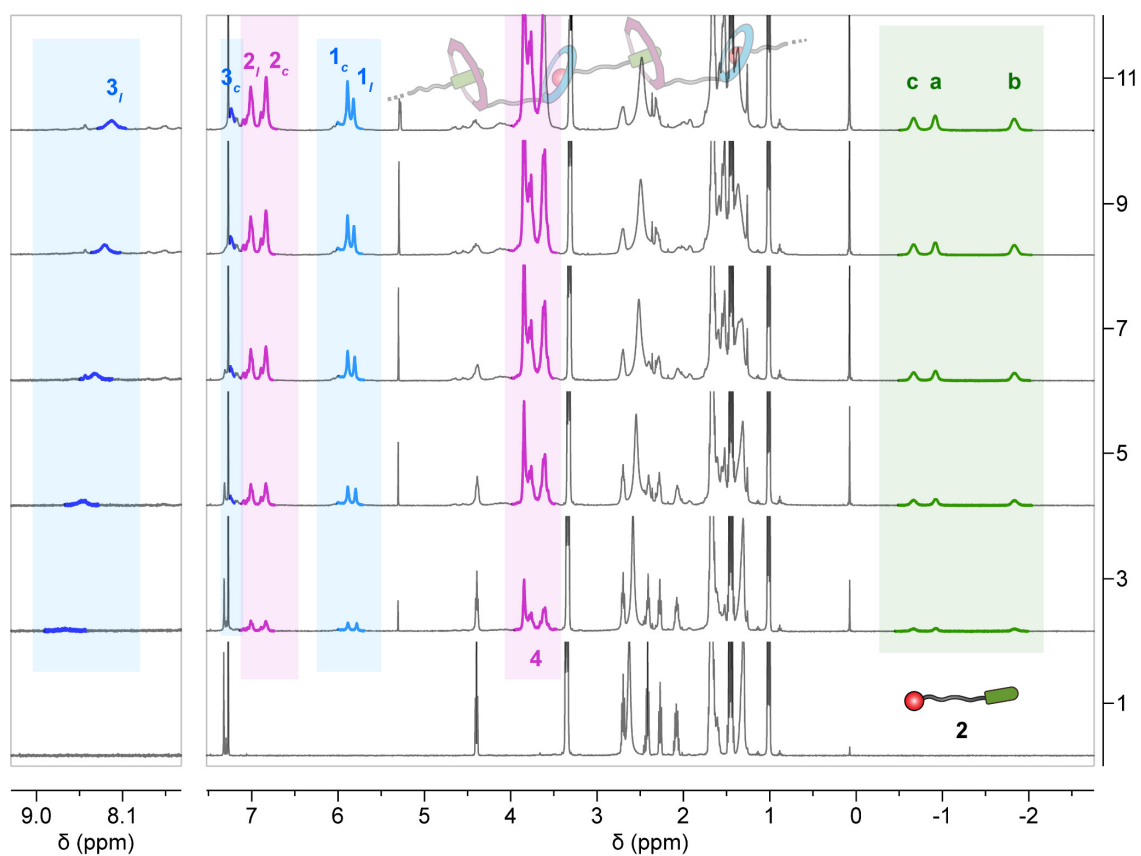


Figure S14. ^1H NMR spectra recorded in CDCl_3 (500 MHz) showing the changes on C4P, P5A, and alkylnitrile peaks during the titration of **2** (10 mM) with incremental amount of **1**. From bottom to top the equivalent of **1** increases in the order of 0.0, 0.2, 0.4, 0.6, 0.8, and 1.0.

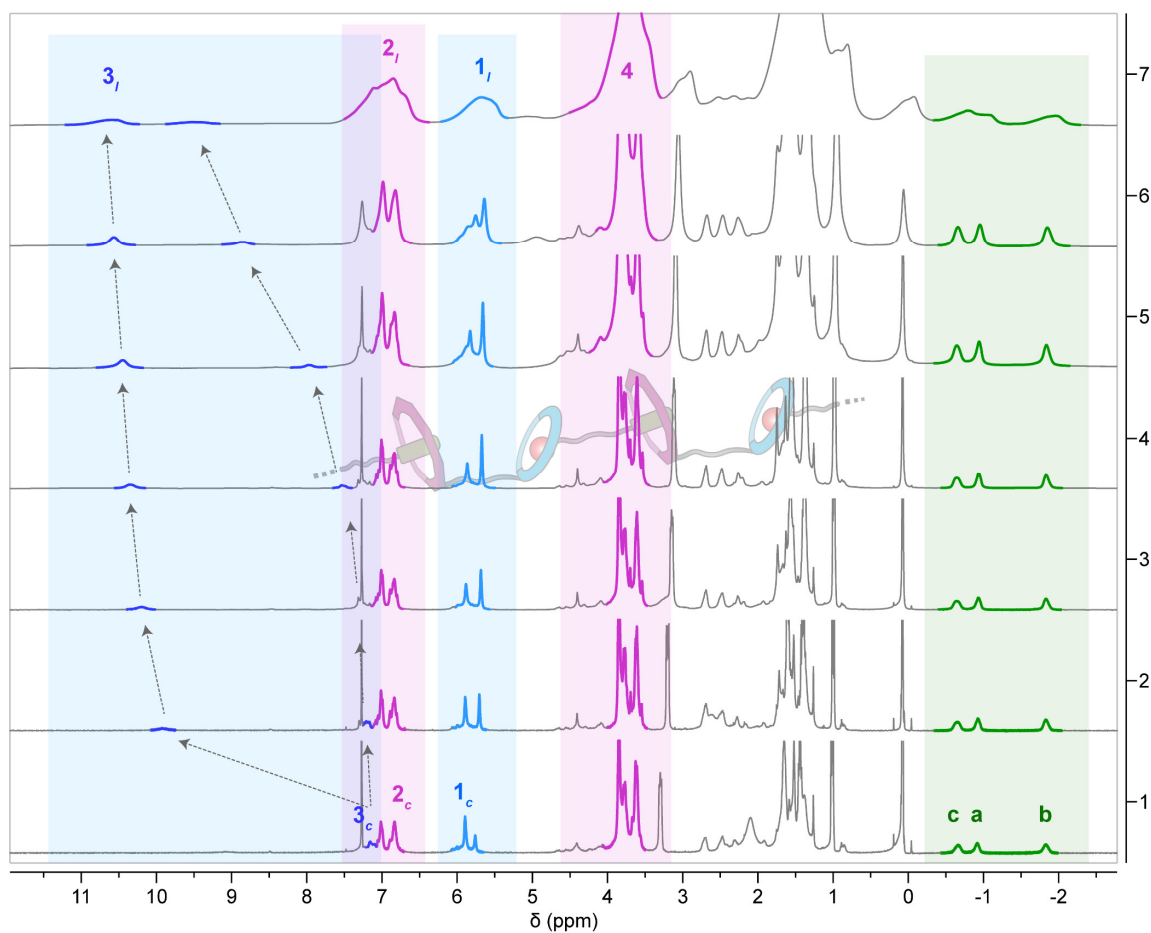


Figure S15. ^1H NMR spectra, recorded in CDCl_3 (500 MHz), showing the peak broadenings and chemical shift changes upon increasing the concentration of **SP**. From bottom to top the concentration of **SP**: 5, 10, 20, 40, 80, 160, and 233 mM.

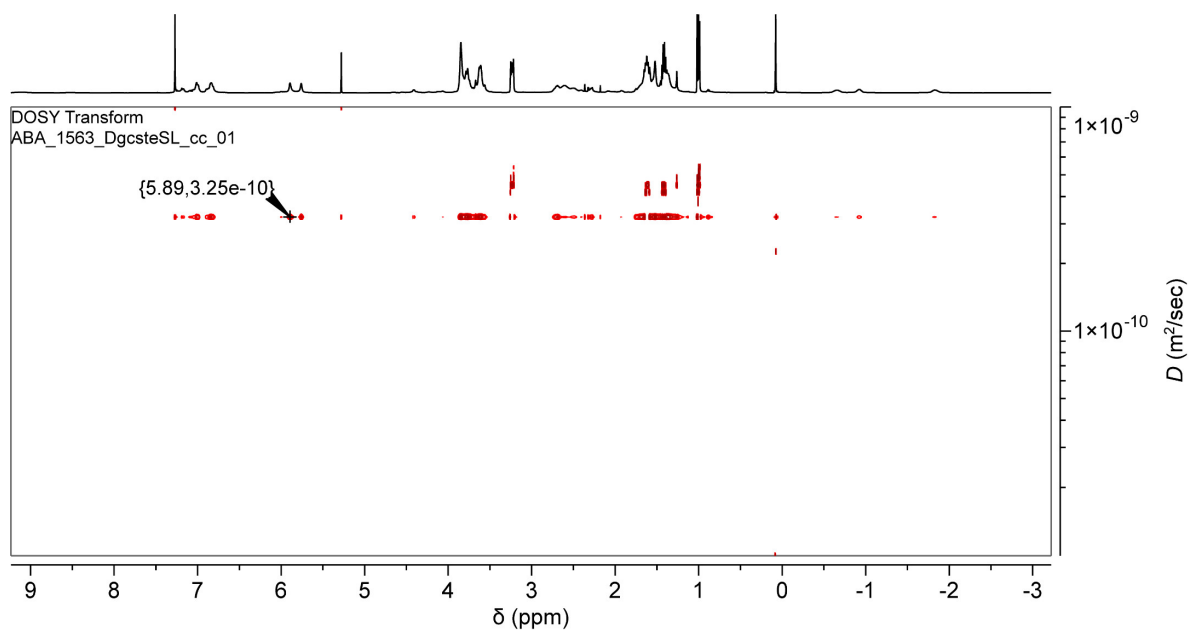


Figure S16. DOSY NMR spectrum of **SP** (10 mM) recorded in CDCl_3 (500 MHz, 25 °C).

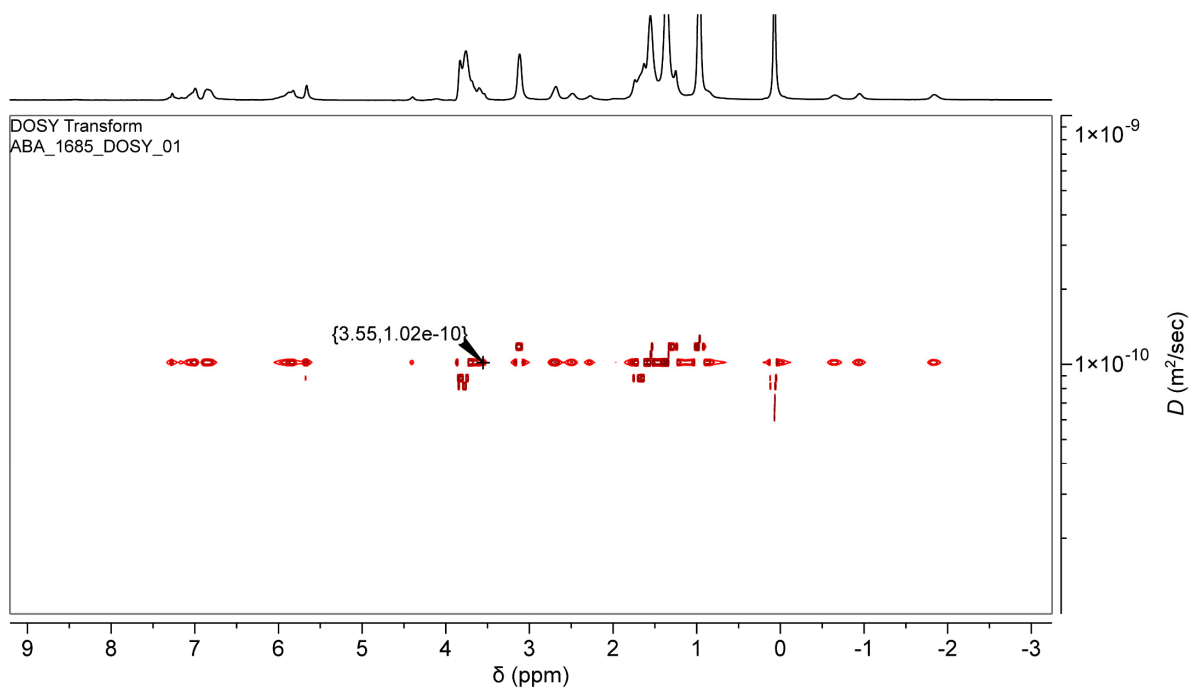


Figure S17. DOSY NMR spectrum of **SP** (100 mM) recorded in CDCl_3 (500 MHz, 25 °C).

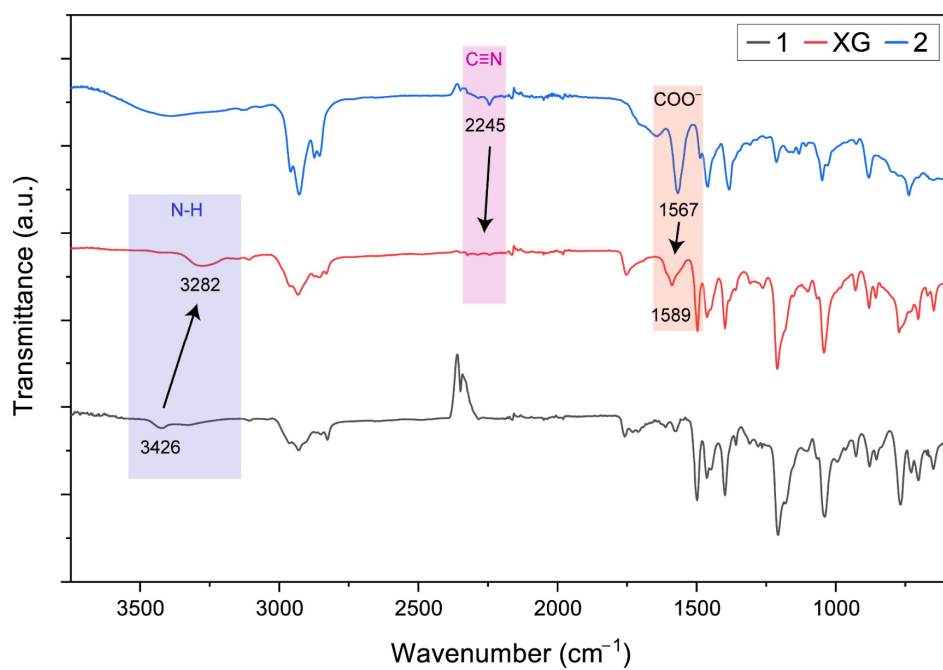


Figure S18. FTIR spectra of the supramolecular monomers **1**, **2**, and **XG**.

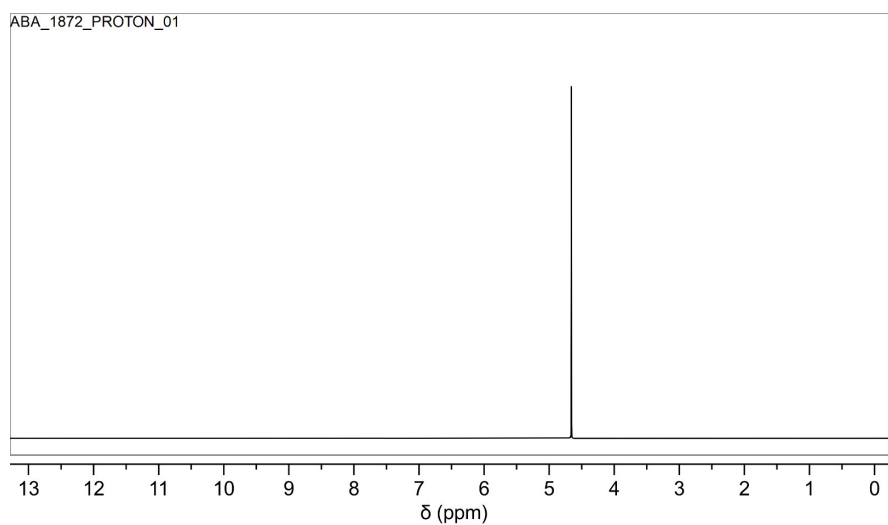


Figure S19. ^1H NMR spectrum of supernatant after treatment of **XG** with D_2O (500 MHz).

Surface Area and Porosity Analysis

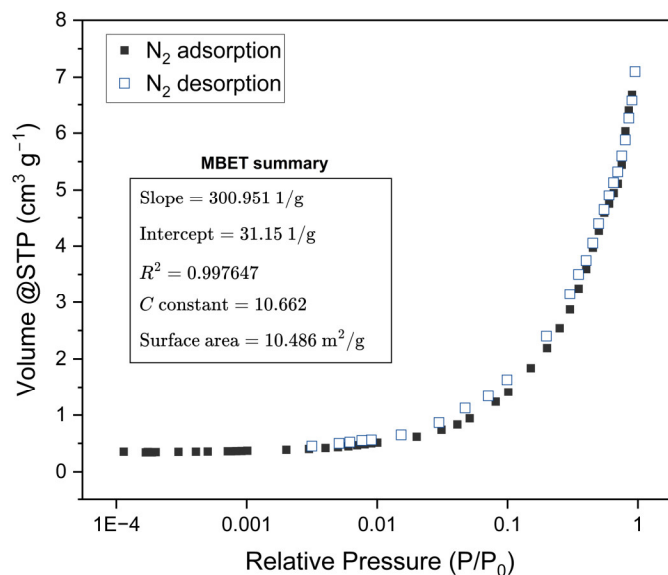


Figure S20. N_2 adsorption (solid symbols) and desorption (open symbols) isotherms at 77.35 K of XG.

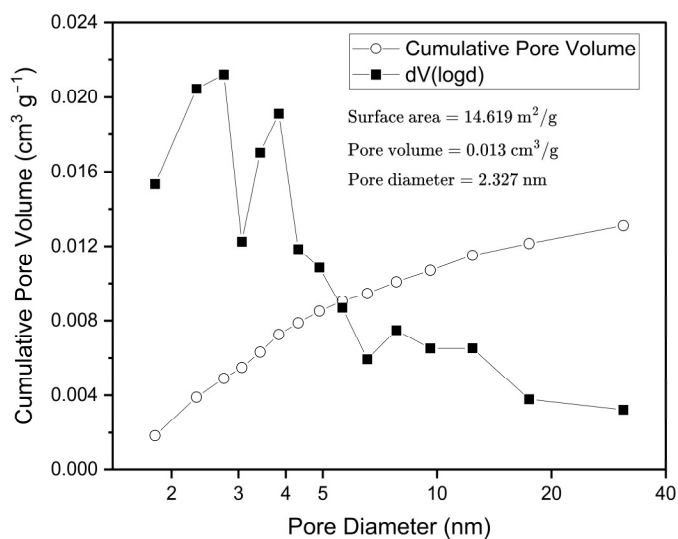


Figure S21. BJH desorption analysis plot of XG.

Micropollutant Removal

Adsorption experiments

Experiments for pollutant removal were conducted at room temperature (25.0 °C) in an aqueous environment using 1-naphthol (1N), 2-naphthol (2N), 1-naphthyl amine (1NA), and 2-naphthylamine (2NA), bisphenol A (BPA), methylene blue (MB), methyl orange (MO), rhodamine B (RB), Fluorescein sodium (FL), methyl violet (MV), paraquat (PQ), diquat (DQ), as organic micropollutants. For studies involving **XG**, the supramolecular polymer xerogel (5.00 mg) was initially cleansed with deionized water for 5.00 minutes and subsequently filtered using Whatman filter paper. Subsequently, **XG** was transferred to a 10.0 mL vial. A pollutant stock solution (0.100 mM, 5.00 mL) was then added to the flask. The mixture was promptly transferred to a shaker, and at predetermined intervals, 1.00 mL of the sample from the flask was taken using a calibrated syringe, diluted with a certain amount of deionized water (dilution factors are 2.5 for 1N and 2N, 6.0 for the other micropollutants), and immediately filtered through a membrane filter. UV/Vis spectroscopy was employed to measure the residual concentration of the pollutant in each sample. The detection wavelengths were determined by the characteristic absorption peak of each sample.

Removal efficiency

The pollutant removal efficiency (in %) by adsorbent **XG** was calculated using this equation:

$$\text{Pollutant removal efficiency (\%)} = \frac{C_0 - C_t}{C_0} \times 100$$

where C_0 (mM) and C_t (mM) are the concentrations of pollutant before and after adsorption, respectively.

The adsorbed pollutant amount was calculated using the following equation:

$$q_t = \frac{(C_0 - C_t) \times M_w}{m}$$

where q_t (mg g⁻¹) is amount of pollutant adsorbed per g of sorbent at time t (min). C_0 (mmol L⁻¹) and C_t (mmol L⁻¹) are the initial and residual concentration of pollutant in the stock solution and filtrate, respectively; m (g) is the mass of sorbent used in the study. M_w (g mol⁻¹) is the molar mass of the pollutant.

Adsorption kinetics

The adsorption kinetics were quantified using the pseudo-first order model,⁴ the pseudo-second order model⁵ and the Weber and Morris intra-particle diffusion model⁶ were employed. These adsorption kinetics are expressed by the following equations:

Model	Equation	Nonlinear curve fit equation	
Pseudo-first order	$\ln(q_e - q_t) = \ln(q_e) - k_1 t$	$q_t = q_e(1 - e^{-k_1 t})$	S1
Pseudo-second order	$\frac{t}{q_t} = \frac{t}{q_e} + \frac{1}{k_2 q_e^2}$	$q_t = \frac{t}{\frac{t}{q_e} + \frac{1}{k_2 q_e^2}}$	S2
Weber and Morris	$q_t = k_i t^{1/2} + C$		S3

where q_t (mg g⁻¹) is the amount of dye adsorbed by the adsorbent at time t (min); q_e (mg g⁻¹) is the amount of dye adsorbed by the adsorbent at equilibrium, respectively, k_1 (min⁻¹); k_2 (g mg⁻¹ min⁻¹) and k_i (mg g⁻¹ min^{0.5}) stand for the pseudo-first-order model, the pseudo-second-order model and the Weber and Morris intra-particle diffusion model rate constants, respectively; C represents a constant related to the thickness of the boundary layer. The constants mentioned here can be determined by performing a nonlinear or linear fit of the experimental data using the appropriate model.

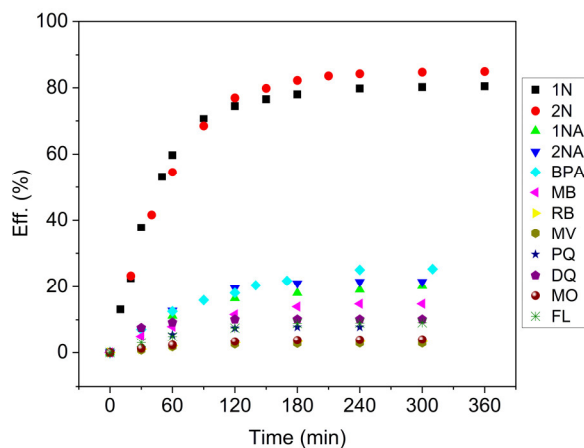


Figure S22. Micropollutant removal efficiencies of **XG** based on the proper calculations from micropollutant calibration curves.

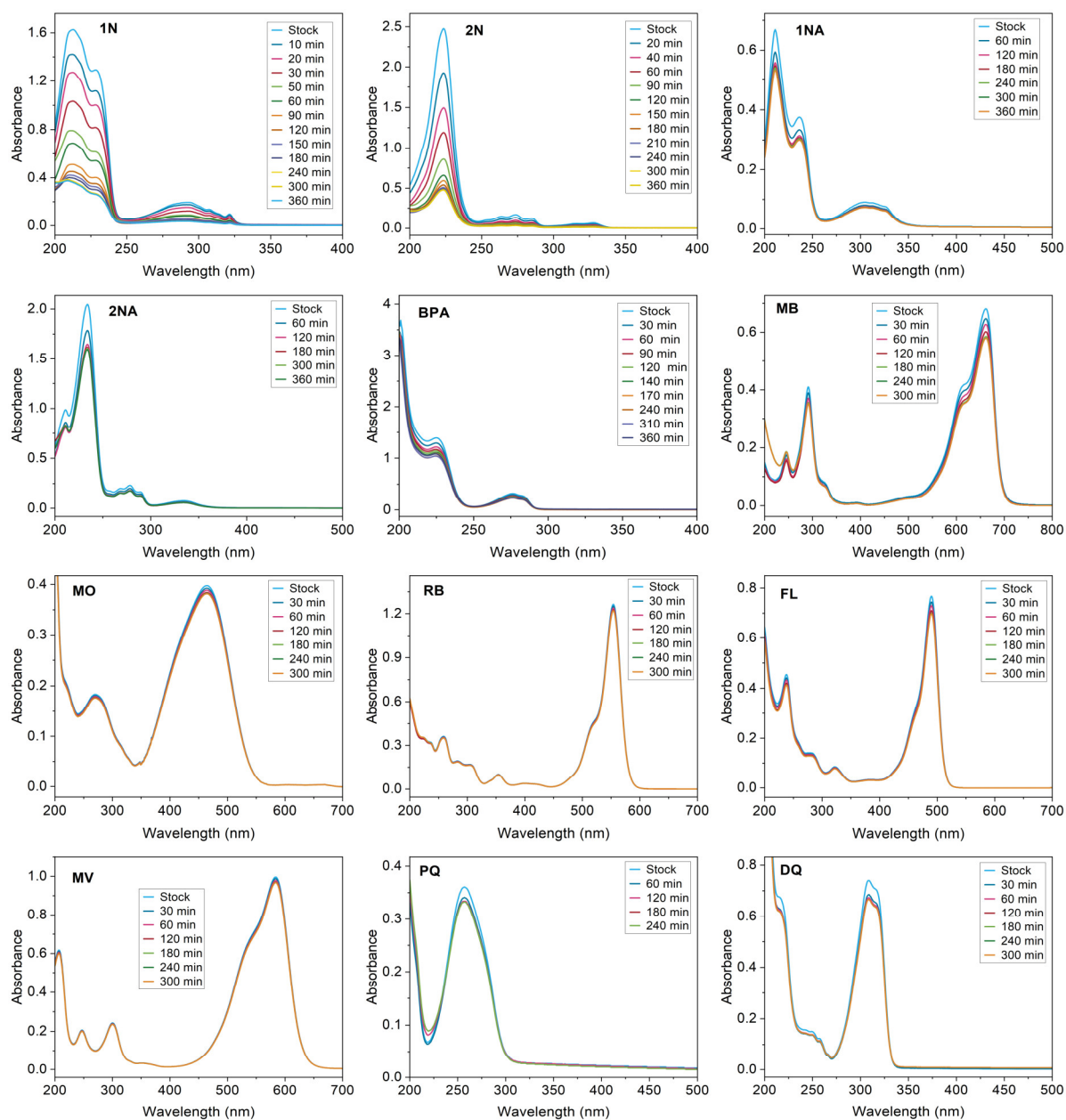


Figure S23. UV/Vis absorption spectra of aqueous solutions of organic micropollutants (0.1 mM) in the presence of XG (1.0 mg mL⁻¹) recorded as a function of increasing adsorption times.

Table S1. Rate parameters and nonlinear regression correlation coefficients of the pseudo-first-order model, the pseudo-second-order model and the Weber and Morris intraparticle diffusion model of **XG** in adsorptions.

Entry	Pseudo-first order model				Pseudo-second order model		Weber and Morris model			
	<i>Eff.</i> %	<i>qe</i> mg/g	<i>k</i> ₁ min ⁻¹	<i>R</i> ²	<i>k</i> ₂ g mg ⁻¹ min ⁻¹	<i>R</i> ²	<i>k</i> _{i1} mg g ⁻¹ min ^{1/2}	<i>R</i> ²	<i>k</i> _{i2} mg g ⁻¹ min ^{1/2}	<i>R</i> ²
1N	80.5	11.56	0.02099	0.99573	0.00431	0.88904	1.37607	0.98517	0.10165	0.8835
2N	84.8	11.8	0.01765	0.99824	0.00347	0.89143	1.16183	0.9915	0.05989	0.81756
1NA	20.3	2.9	0.01338	0.9985	0.01138	0.96108				
2NA	22.1	3.2	0.01565	0.99649	0.01296	0.95527				
BPA	25.3	5.8	0.01142	0.99469	0.00393	0.92179				
MB	14.8	4.7	0.01353	0.99606	0.01271	0.92967				
MO	4.0	1.3	0.01464	0.99755	0.02209	0.9307				
RB	3.4	1.63	0.01531	0.98741	0.01862	0.90243				
FL	9.1	3.42	0.01415	0.99414	0.0082	0.92015				
MV	2.9	1.2	0.01549	0.98589	0.02571	0.90414				
PQ	7.8	2.0	0.02199	0.99697	0.03461	0.9683				
DQ	10.1	3.5	0.04471	0.99925	0.03861	0.98824				

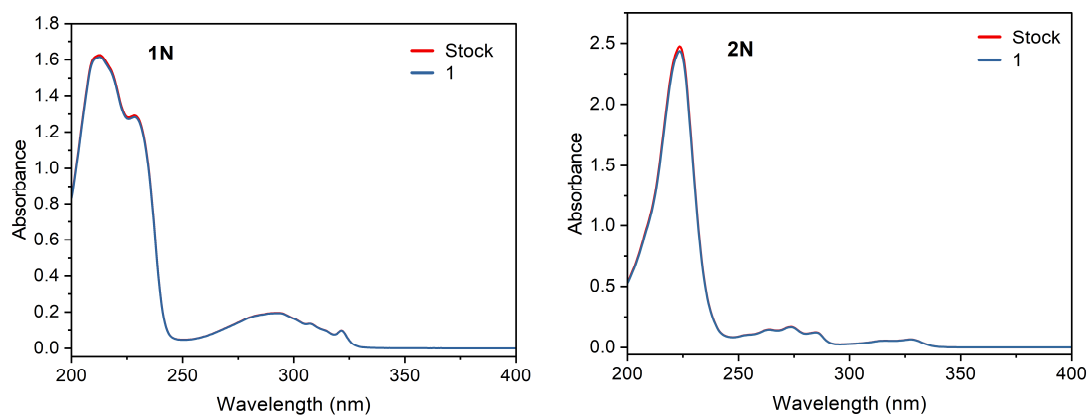


Figure S24. UV/Vis spectra showing the inefficient micropollutant uptake performance of the supramolecular monomer **1** (1 mg/mL) after 3 h contact with 5 mL **1N** and **2N** solutions (0.1 mM).

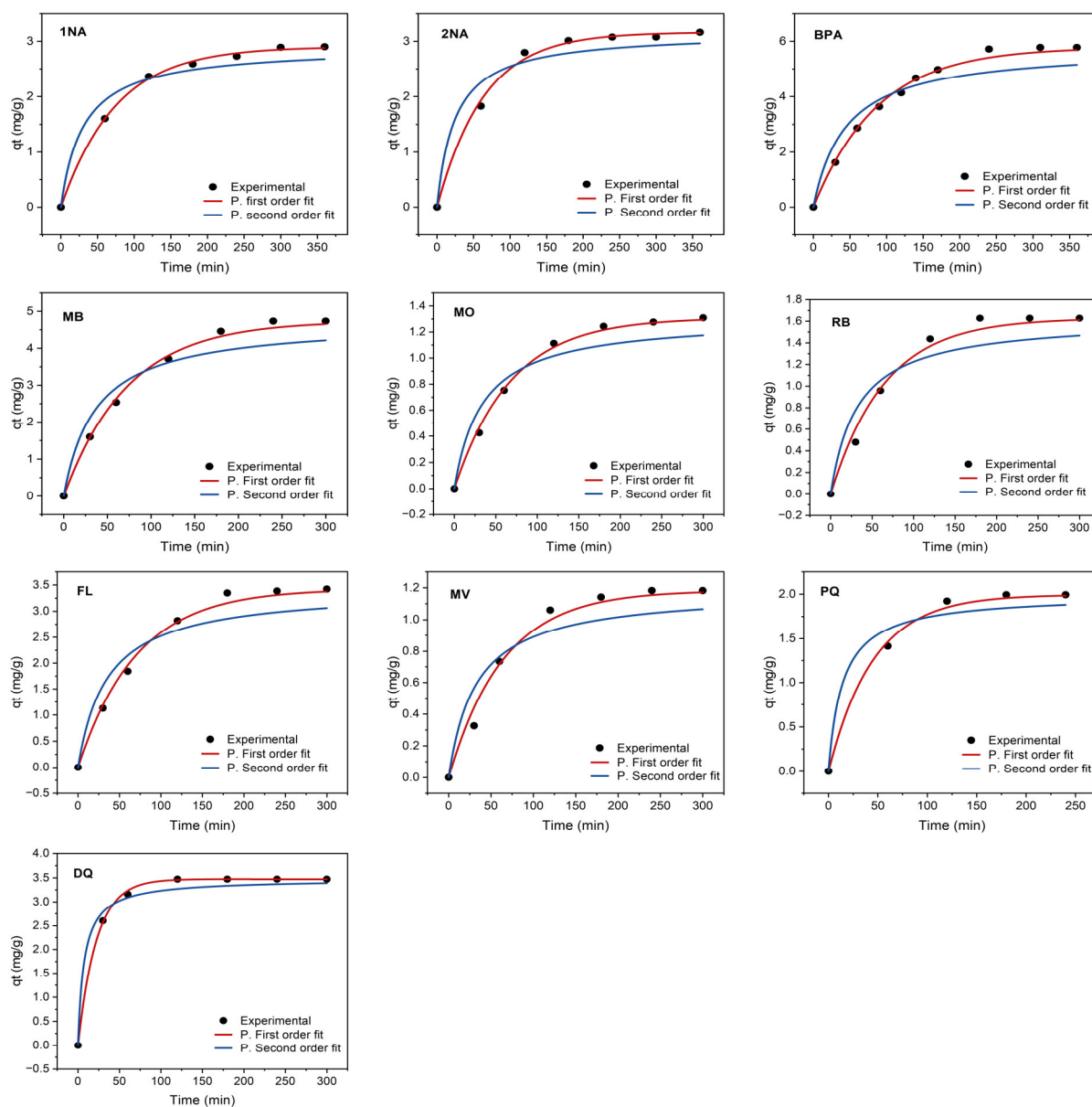


Figure S25. Pseudo-first- and pseudo-second-order nonlinear curve fits of XG for organic micropollutants studied.

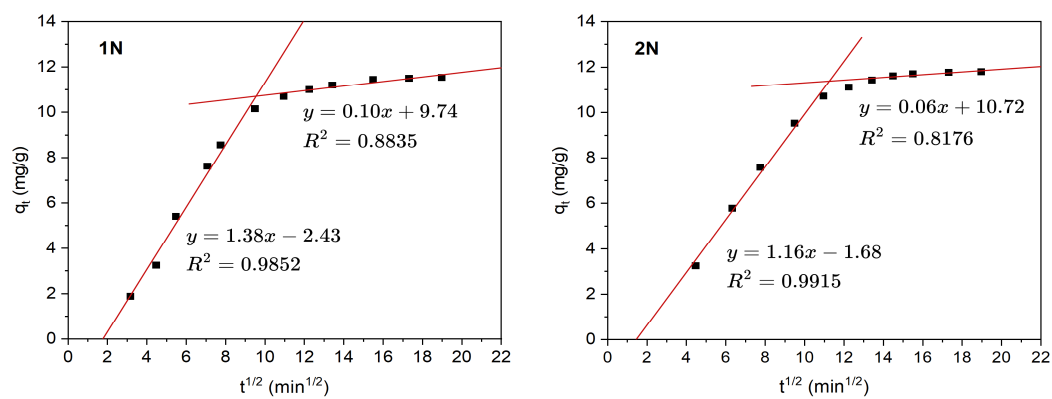


Figure S26. Fits to Weber and Morris intra-particle diffusion model for **1N** and **2N** uptakes by **XG**.

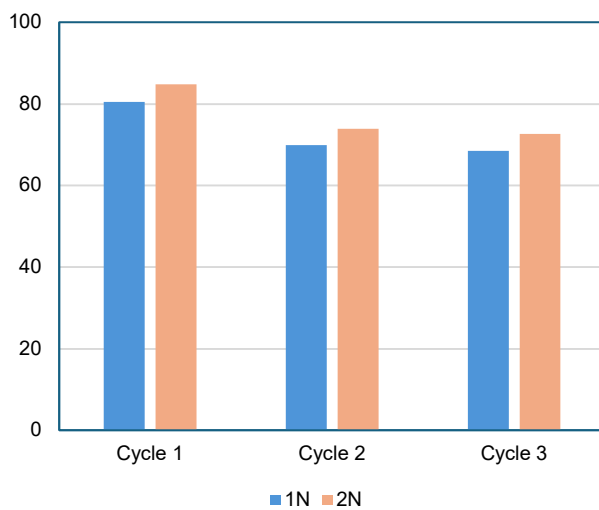


Figure S27. **1N** and **2N** removal efficiencies by **XG** after consecutive regeneration cycles.

Adsorption isotherms

The adsorption isotherm was described using the Langmuir adsorption isotherm model.⁷ The corresponding isotherm parameter can be calculated using the following equation:

$$\frac{C_e}{q_e} = \frac{1}{q_{max}K} + \frac{C_e}{q_{max}}$$

where K stands for the Langmuir constant, and q_{max} (mg g⁻¹) is the maximum adsorption amount, C_e (mg L⁻¹) is the residual dye concentrations of the dye adsorbed by **XG** at equilibrium and q_e (mg g⁻¹) is the amount of dye adsorbed by **XG** at equilibrium. All the constants mentioned above can be calculated by the linear fitting of the experimental data using the isotherm model. See main text Fig. 2 for the corresponding isotherm graphics.

We also utilized the empirical Freundlich adsorption isotherm model.^{8,9} The isotherm parameters in question can be determined by applying the following equation:

$$\ln Q_e = \ln K_f + \frac{1}{n} \ln C_e$$

In this equation, K_f represents the Freundlich equilibrium constant (mg/L), while n indicates the energy heterogeneity of adsorption sites, reflecting the nonlinearity between solution concentration and adsorption. See main text Fig. 2 for the corresponding isotherm graphics.

Table S2. The adsorption isotherm parameters derived from fitting isotherm models to the experimental data of **XG** in the adsorption process.

Micropollutant	Langmuir isotherm model			Freundlich isotherm model		
	K_L (L mg ⁻¹)	q_{max} (mg g ⁻¹)	R_2	K_F (L mg ⁻¹)	n	R^2
1N	6665	108.7	0.9952	4.78	1.09	0.9844
2N	8426	122.6	0.9943	6.62	1.12	0.9884

Binary-Component Adsorptions

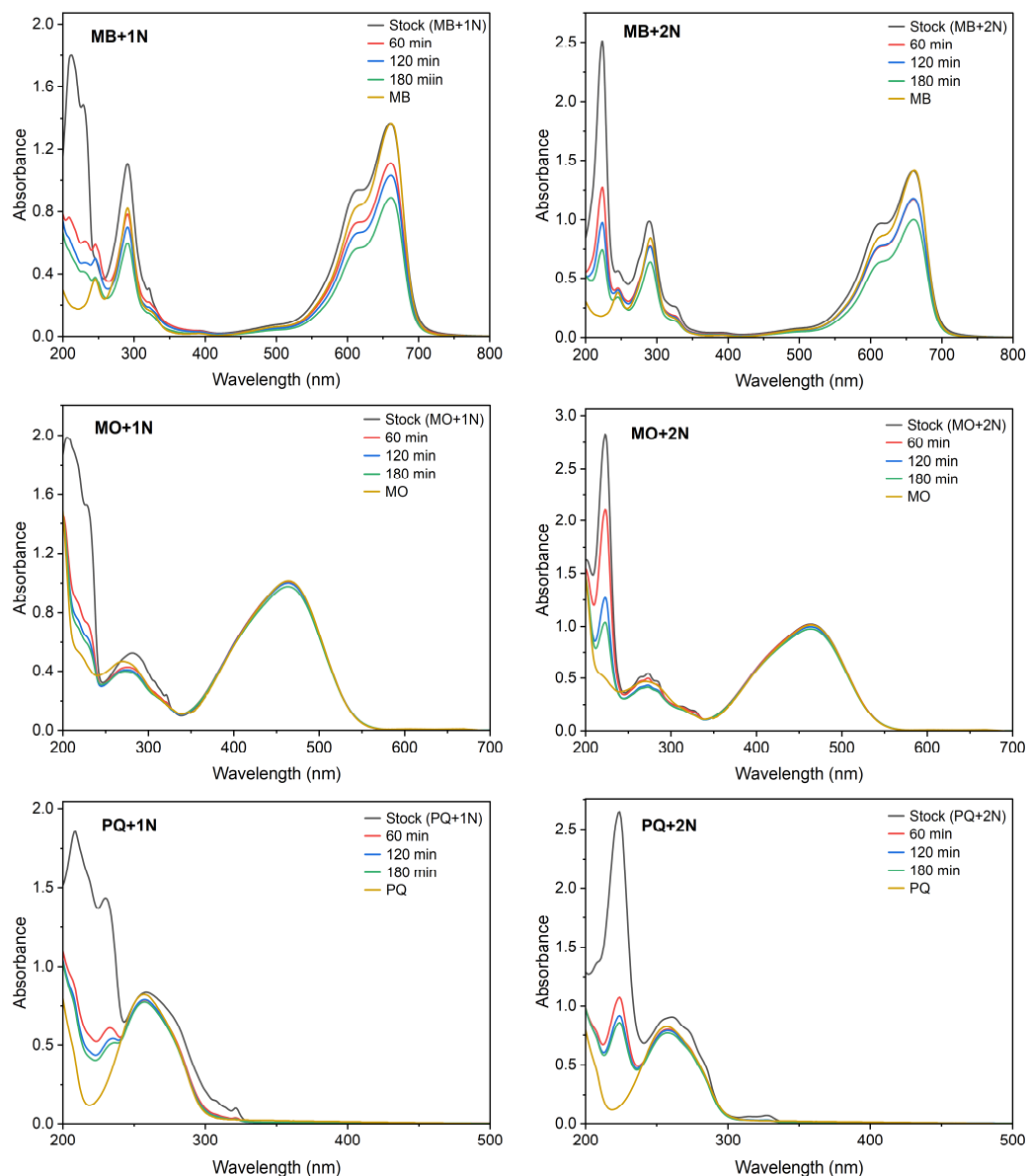


Figure S28. UV/Vis absorption spectra belonging to aqueous solutions of binary mixtures of organic micropollutants (0.1 mM each) in the presence of **XG** (1.0 mg mL^{-1}) recorded as a function of increasing adsorption times (0, 60, 120, and 180 min). Second components (MB, MO, and PQ) were also included in the spectra for comparison.

The ability of **XG** to adsorb **1N** and **2N** selectively from aqueous binary organic micropollutant mixtures containing equimolar MB, MO and PQ were carried out similar to kinetic experiments. For instance, an **XG** sample (1 mg mL^{-1}) was added to an equimolar mixture of **1N** and MB (0.1 mM) and supernatants (1 mL) were taken at certain time intervals from adsorption medium. After dilution of the sample to 2.5 mL UV/Vis measurements were carried out (Figure S27). Other binary

components were also analyzed under the same conditions. Efficiency and selectivity results based on UV/Vis analyses can be found at Table S3.

Table S3. Removal efficiency and selectivity data belonging to binary-components after 180 min.

1N efficiencies			Second component efficiencies				
	Eff. (%)	Change (%)		Eff. (%)		Eff. (%)	Change (%)
1N only	75.65						
1N + MB	72.22	−3.43	MB only	13.95	1N + MB	27.01	+13.06
1N + MO	74.53	−1.12	MO only	3.77	1N + MO	3.65	−0.12
1N + PQ	72.95	−2.70	PQ only	7.76	1N + PQ	7.41	−0.35

2N efficiencies			Second component efficiencies				
	Eff. (%)	Change (%)		Eff. (%)		Eff. (%)	Change (%)
2N only	77.97						
2N + MB	76.70	−1.27	MB only	13.95	2N + MB	28.98	+15.03
2N + MO	75.99	−1.98	MO only	3.77	2N + MO	4.50	+0.73
2N + PQ	74.23	−3.74	PQ only	7.76	2N + PQ	7.78	+0.02

References

1. Y.-F. Zhang, Y.-J. Li, Z.-H. Wang, X.-W. Sun, Q.-Y. Yang, H.-Q. Dong, Y.-M. Zhang, T.-B. Wei, H. Yao and Q. Lin, *Journal of Materials Chemistry C*, 2021, **9**, 10347-10353.
2. D. Memis, N. Bektas and A. Aydogan, *ACS Appl. Polym. Mater.*, 2024, **6**, 4339-4348.
3. N. Song, D.-X. Chen, Y.-C. Qiu, X.-Y. Yang, B. Xu, W. Tian and Y.-W. Yang, *Chem. Commun.*, 2014, **50**, 8231-8234.
4. K. L. Tan and B. H. Hameed, *J. Taiwan Inst. Chem. Eng.*, 2017, **74**, 25-48.
5. Y. S. Ho and G. McKay, *Process Biochemistry*, 1999, **34**, 451-465.
6. W. J. Weber and J. C. Morris, *Journal of the Sanitary Engineering Division*, 1963, **89**, 31-59.
7. I. Langmuir, *J. Am. Chem. Soc.*, 1918, **40**, 1361-1403.
8. H. Freundlich and G. Losev, *Zeitschrift für Physikalische Chemie*, 1907, **59U**, 284-312.
9. J. Debord, K. H. Chu, M. Harel, S. Salvestrini and J.-C. Bollinger, *Langmuir*, 2023, **39**, 3062-3071.